

Supplementary Information

Super-Assembled Periodic Mesoporous Organosilica Membranes with Hierarchical Channels for Efficient Glutathione Sensing

Hui Zeng,^a Shan Zhou,^a Xin Zhang,^a Qirui Liang,^a Miao Yan,^a Yeqing Xu,^a Yaxin Guo,^a Xiaomeng Hu,^a Lei Jiang^b and Biao Kong^{a,c,d}*

^a Department of Chemistry, Shanghai Key Lab of Molecular Catalysis and Innovative Materials and Collaborative Innovation Center of Chemistry for Energy Materials, Fudan University, Shanghai 200438, P. R. China

^b CAS Key Laboratory of Bio-Inspired Materials and Interfacial Science, Technical Institute of Physics and Chemistry, Chinese Academy of Science, Beijing 100190, P. R. China

^c Yiwu Research Institute of Fudan University, Yiwu, Zhejiang 322000, P. R. China

^d Shandong Research Institute, Fudan University, Jinan, Shandong 250103, P. R. China

* Corresponding author: Biao Kong (B.K.)

Email address: bkong@fudan.edu.cn

Table of contents

Fig. S1	TEM image of the mesostructured organic-inorganic hybrid nanoparticles before structural transformation
Fig. S2	SEM images of the PMOs
Fig. S3	FT-IR spectra of the PMOs
Fig. S4	^{29}Si MAS NMR spectra of the PMOs
Fig. S5	Optical image of the pure AAO
Fig. S6	SEM images of the pure AAO
Fig. S7	SEM images of the PMO/AAO with 25 wt % loading of PMOs
Fig. S8	SEM images of the PMO/AAO with 30 wt % loading of PMOs
Fig. S9	SEM images of the PMO/AAO with 35 wt % loading of PMOs
Fig. S10	SEM images of the PMO/AAO with 45 wt % loading of PMOs
Fig. S11	Effect of temperature and pH on the detection of GSH
Table S1	Sensing of GSH in FBS samples

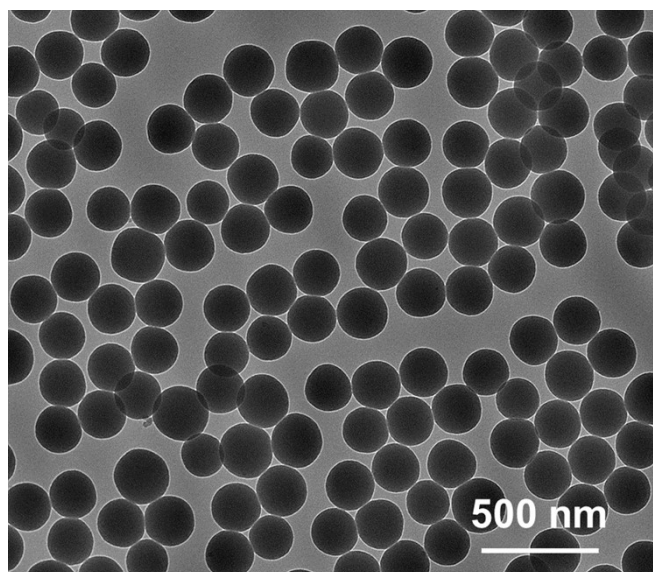


Fig. S1 TEM image of the mesostructured organic-inorganic hybrid nanoparticles before structural transformation.

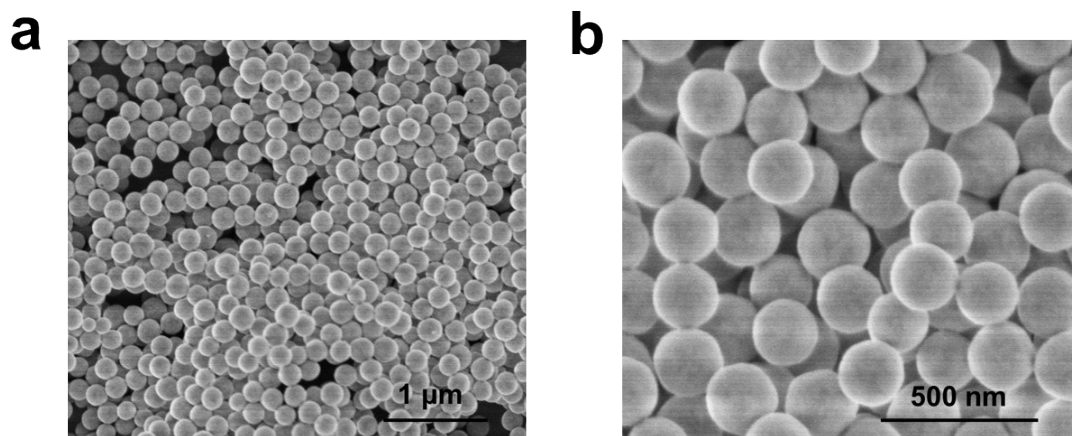


Fig. S2 SEM image (a) and magnified view (b) of the thioether-bridged PMOs with yolk-shell structure.

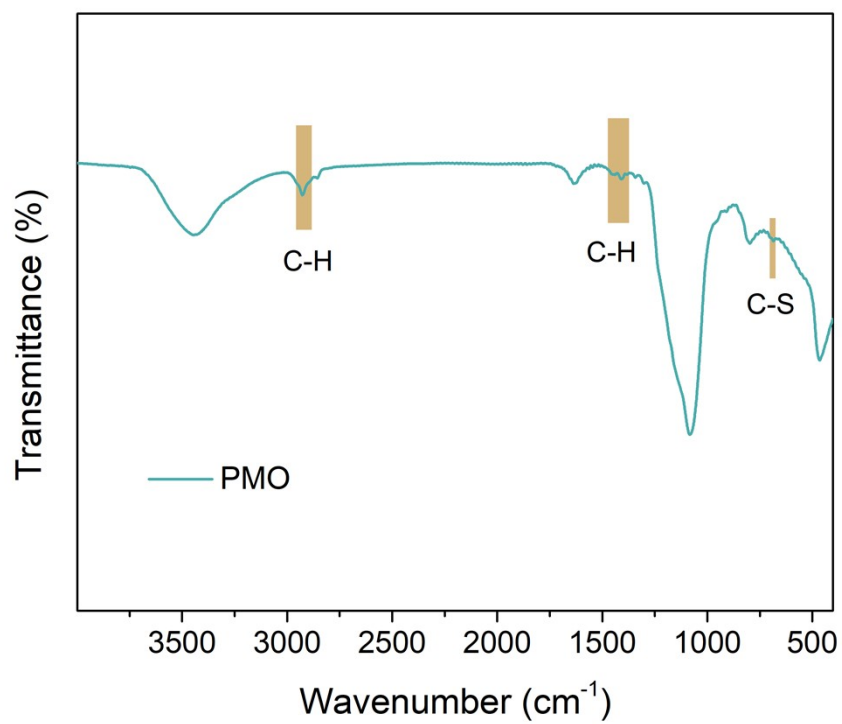


Fig. S3 FT-IR spectra of as-made PMOs.

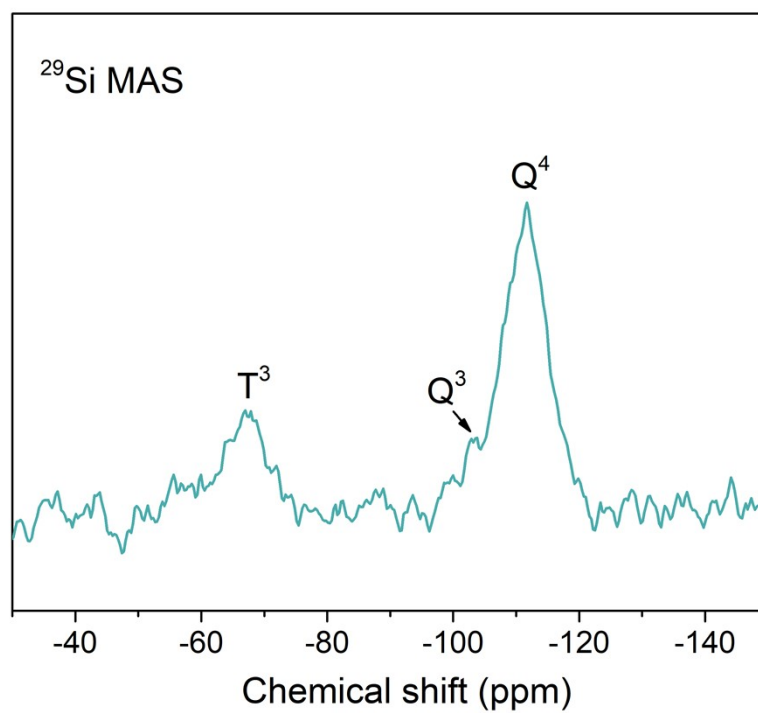


Fig. S4 ^{29}Si MAS NMR spectra of as-made PMOs.

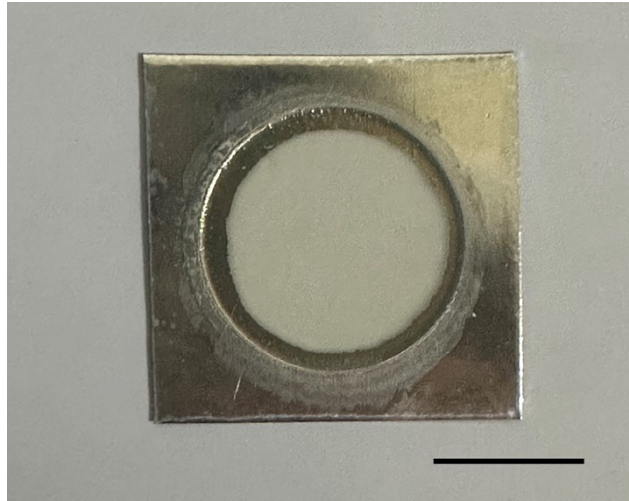


Fig. S5 Optical image of the pure AAO (Scale is 1 cm).

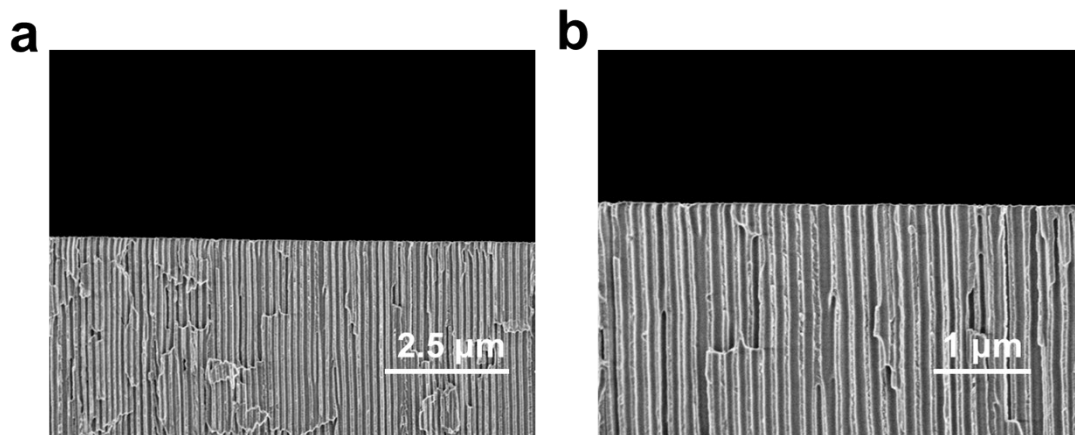


Fig. S6 Cross-sectional SEM images (a, b) of the AAO membrane.

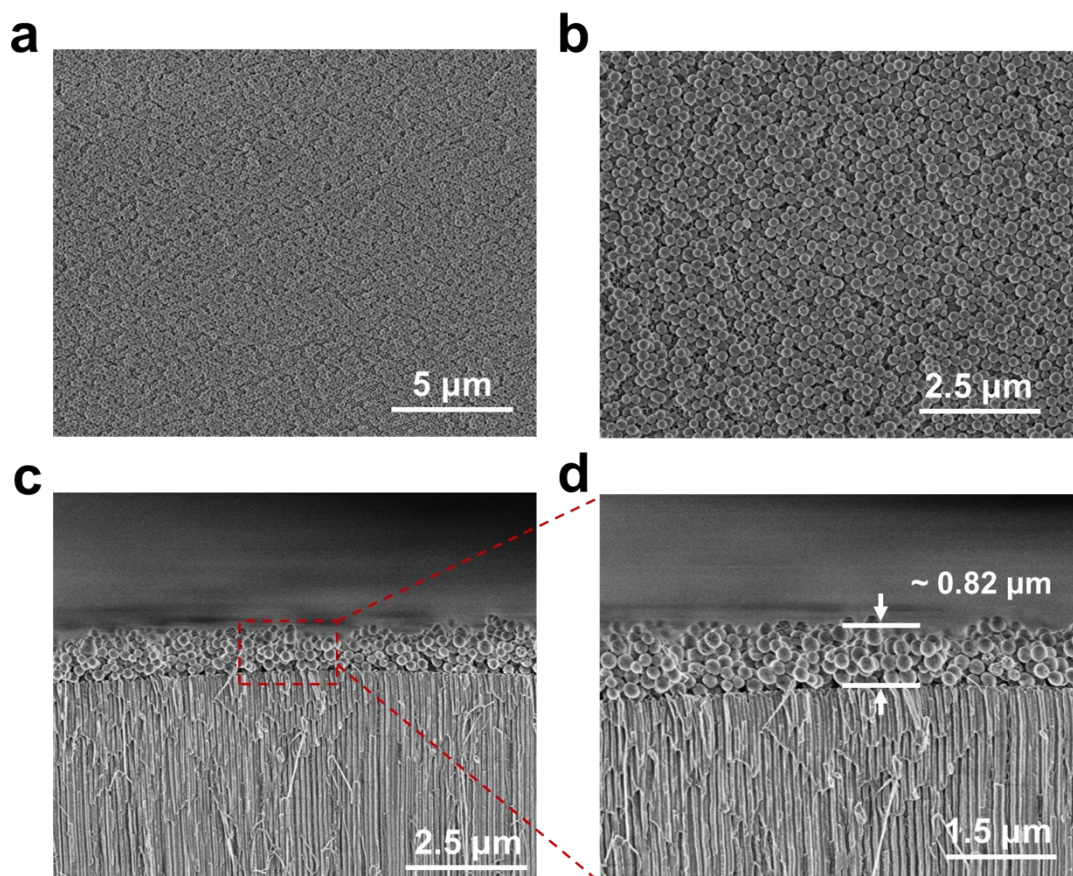


Fig. S7 Surface SEM images (a, b) and cross-sectional images (c, d) of the PMO/AAO membrane with 25 wt % loading of PMOs.

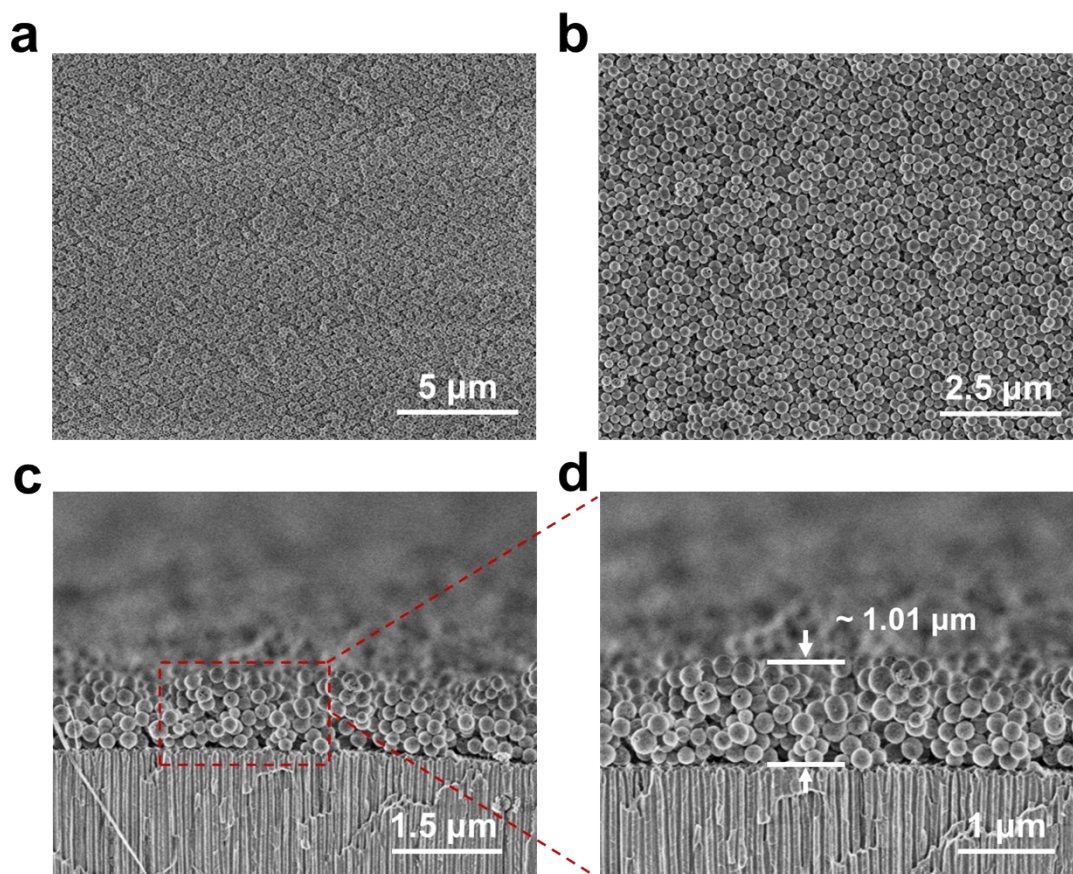


Fig. S8 Surface SEM images (a, b) and cross-sectional images (c, d) of the PMO/AAO membrane with 30 wt % loading of PMOs.

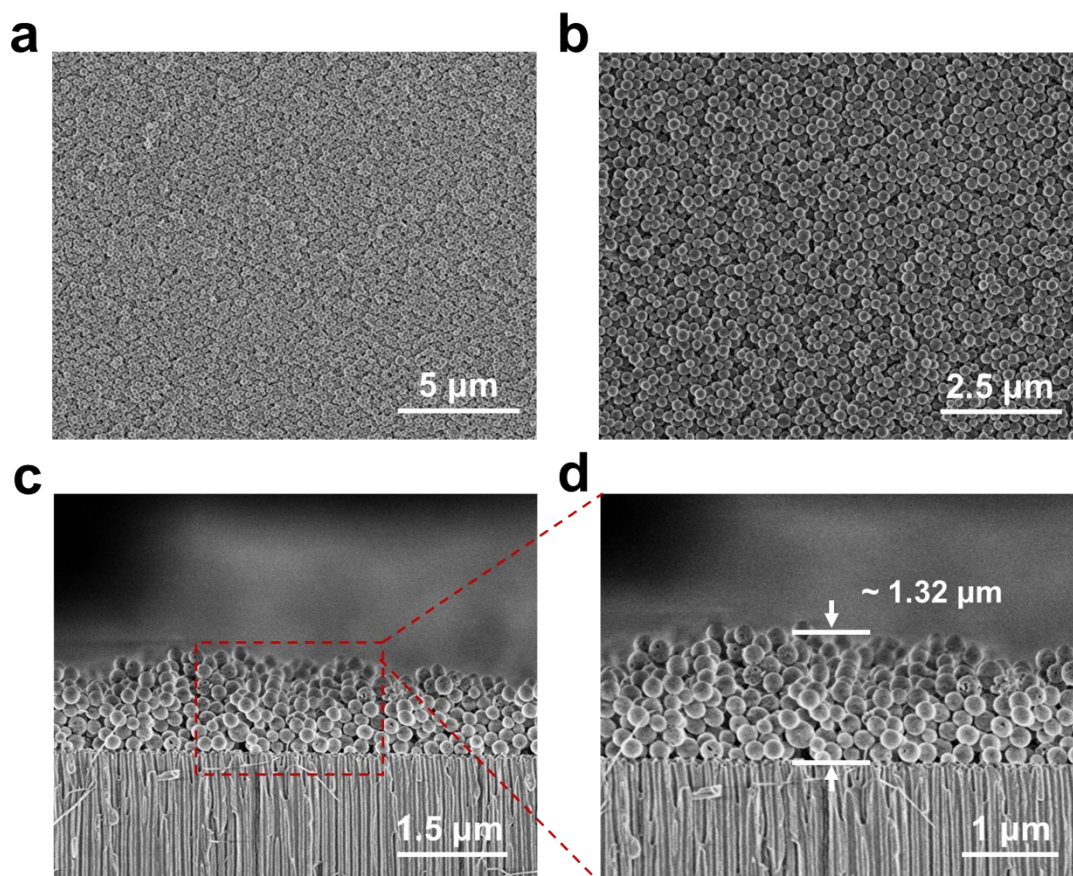


Fig. S9 Surface SEM images (a, b) and cross-sectional images (c, d) of the PMO/AAO membrane with 35 wt % loading of PMOs.

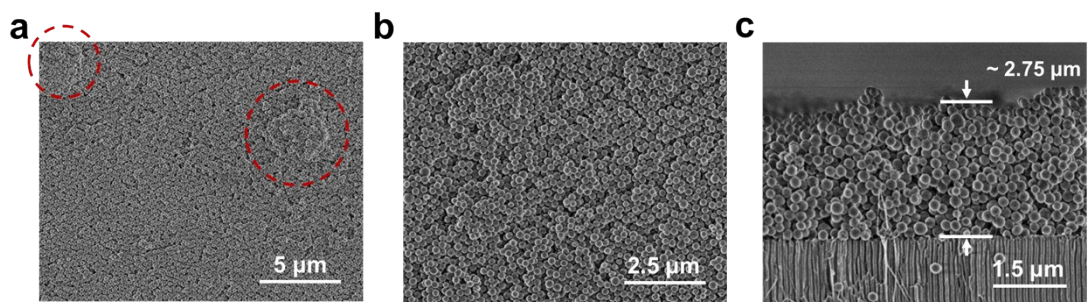


Fig. S10 Surface SEM images (a, b) and cross-sectional image (c) of the PMO/AAO membrane with 45 wt % loading of PMOs.

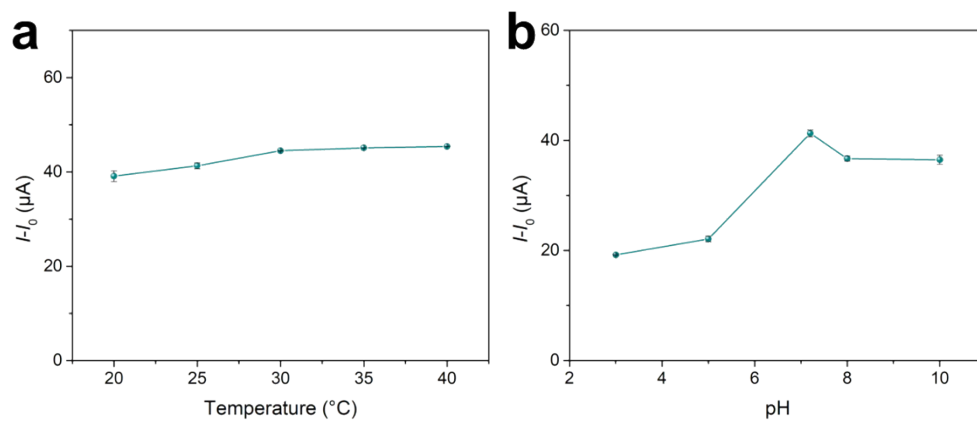


Fig. S11 (a) Effect of temperature on the detection of GSH (10 mM, pH = 7.2, 60 min).

(b) Effect of pH on the detection of GSH (10 mM, T = 25 $^{\circ}\text{C}$, 60 min).

Table S1 Sensing of GSH in FBS samples

Added (mM)	Founded^a (mM)	Recovery^b (%)
0.05	0.045 ± 0.006	90.6
0.1	0.118 ± 0.098	118.4

^aMean and standard deviation (SD) of the results (n = 3)

^bRecovery (%) = $C_{\text{GSH founded}} / C_{\text{GSH added}} * 100$